Resolving sea level contributions by identifying fingerprints in time-variable gravity and altimetry

R. Rietbroek[a], S.-E. Brunnabend[b], J. Kusche[a], J. Schröter[b]

[a] *Institute of Geodesy and Geoinformation, Bonn University, Bonn, Germany*
[b] *Alfred Wegener Institute for Polar and Marine Research, Bremerhaven, Germany*

Abstract

We have studied the ability of the GRACE gravimetry mission and Jason-1 altimetry to resolve ice and glacier induced contributions to sea level rise, by means of a fingerprint method. Here, the signals from ice sheet and land glacier changes, steric changes, glacial isostatic adjustment and terrestrial hydrology are assumed to have fixed spatial patterns. In a joint inversion using GRACE and Jason-1 data the unknown temporal components can then be estimated by least-squares. In total, we estimate temporal components for up to ~80 individual patterns. From a propagation of the full error-covariance from GRACE and a diagonal error-covariance from Jason-1 altimetry we find that: 1) GRACE almost entirely explains the mass related parameters in the joint inversion, 2) An inversion using only Jason-1 data has a marginal ability to estimate the mass related parameters, while the steric parameters have much better formal accuracy. In terms of mean sea level rise the steric patterns have a maximum formal accuracy of 0.01 mm for an 11 week running mean. In general, strong negative error correlations (<-0.9) exists between the high and low elevation parts of the ice sheet drainage basins, when those are estimated independently. The largest formal errors found are in the order of 40 Gton for small high elevation subbasins in the southern Greenland ice sheet, which are difficult to separate. In a simplified joint inversion, merging high and low elevation basins, we have investigated the ability of the GRACE and Jason-1 data to separate the geocenter motion into a present-day contribution and a contribution from glacial isostatic adjustment (GIA). We find that the GIA related signal is larger than the present-day component with a maximum of -0.71 mm/yr in the Z direction. Total geocenter motion rates are found to be -0.28, 0.43, -1.08 mm/yr for the X, Y and Z components respectively. The inversion results have been propagated to the Jason-1 along-track measurements. Over the time period considered, we see that a large part of the variability in the Pacific, Atlantic and Indian ocean can be explained by our inversion results. The applied inversion method therefore seems a feasible way to separate steric from mass induced sea level changes. At the same time, the joint inversion would benefit from more advanced parameterizations, which may aid in fitting remaining signal from altimetry.

Keywords: GRACE, Jason-1 altimetry, Sea level rise, geocenter motion

1. Introduction

The recent Intergovernmental Panel on Climate Change 4th assessment report (Bindoff et al., 2007) identified sea level change, although occurring with considerable regional variations, as one of the most important environmental problems for the coming century. Sea level rise will affect many countries of the world and a large share of the global population will have to adjust to it. However, predicted sea level change rates still vary significantly, dependent on the choice of climate models used in the predictions.

On the other hand, measured contemporary sea level provides a sensitive and readily accessible indicator of the climate system and its variability and can thus be used to validate our current knowledge and models. Contributors to the currently observed global sea level rise of about 3 mm/year include ice sheet melting in Antarctica and Greenland, melting of glaciers, expansion of the ocean due to warming, changes in the land-ocean and atmosphere-ocean branches of the hydrological cycle. Even glacial isostatic adjustment (GIA), the solid-Earth response to past deglaciation, affects sea level at a significant level. At inter-annual

Email address: roelof@geod.uni-bonn.de (R. Rietbroek)

time scales, phenomena such as El Niño contribute to regional sea level changes. Contrary to common belief, and of crucial importance for this study, all these contributions exhibit a dedicated spatial signature in sea level rather than adding up as uniform layers (Plag and Jüttner, 2001; Mitrovica et al., 2001; Tamisiea et al., 2001).

Antarctica and Greenland estimates of ablation are nowadays mainly based upon spaceborne gravimetry. Both ice sheets currently contribute around $0.5\,{}^{\mathrm{mm}}\!/_{\mathrm{yr}}$ to global sea level rise with considerable variations between studies (Cazenave and Llovel, 2010). A recent study by Wu et al. (2010), based on joint inversion of multiple space-geodetic data sets, estimated the Greenland contribution to sea level rise at just $0.3\,{}^{\mathrm{mm}}\!/_{\mathrm{year}}$. Land glaciers are thought to add a total of $1.4\,{}^{\mathrm{mm}}\!/_{\mathrm{year}}$ (Cogley, 2009), while Cazenave and Llovel (2010) suggest $1.0\,{}^{\mathrm{mm}}\!/_{\mathrm{year}}$ for thermal expansion during 1993-2007 and $0.25\,{}^{\mathrm{mm}}\!/_{\mathrm{year}}$ during 2003-2007. Llovel et al. (2010) conclude that the short-term trend in total land water storage, integrated over the largest river basins of the world, amounts to a small negative contribution to sea level change of $-0.22\,{}^{\mathrm{mm}}\!/_{\mathrm{year}}$.

Present-day ice melting increases the flux of fresh water supplied to the ocean and thus affects salinity on a regional scale (Stammer, 2008; Brunnabend et al., 2011). As a consequence, ocean circulation and sea level respond to it. Little is known quantitatively except from those studies that considered the possibility of a slowdown in the meridional overturning circulation (Willis, 2010).

Stammer (2008) simulated the ocean's response to freshwater forcing by removing salt from the model off the coasts of Greenland and Antarctica. He found that the effect of fresh water forcing from Greenland is mainly restricted to the Atlantic Ocean, but has a sizeable effect on the sea surface height.

More recently, Brunnabend et al. (2011, this issue) forced the Finite Ocean Sea-Ice Ocean Model (FESOM) with meltwater fluxes from Greenland. They ensured mass conservation and studied the effect of both the circulation changes due to fresh water forcing, and the gravitational effect of the dissapearing ice sheet. In addition, a scenario which incorporated seasonal variations of melting was also fed into the model. They found that the salinity and temperature changes were mainly confined to the upper ocean in the Atlantic. Overall rates in sea level change (mass and steric) were found to be approximately proportional to the magnitude of the meltwater flux, with an increase in global sea level of $0.3\,{}^{\mathrm{mm}}\!/_{\mathrm{yr}}$ for $100\,{}^{\mathrm{Gt}}\!/_{\mathrm{yr}}$ of melting in Greenland.

Separating individual sources of sea level rise from tide gauge measurements or satellite altimetry is difficult. Tide gauges are sparse and limited to coastlines, and their measurements need to be corrected for local subsidence and other effects unrelated to sea level. Radar altimetry provides a dense coverage of the oceans, but since Jason-1/TOPEX orbits are confined to latitudes up to 66°, the polar regions cannot be observed. In addition, neither satellite altimetry nor tide gauges are able to distinguish between mass-induced and steric sea level changes.

The Gravity Recovery and Climate Experiment (GRACE) mission has provided researchers with a complete new type of data, leading to a significantly improved knowledge of the mean geoid and of mass redistribution within the oceans. However, the gravitational anomalies measured by GRACE represent mass integrated over a vertical column which is caused by a variety of phenomena within the Earth's interior or on its surface. Several authors have used either ARGO data or GRACE in conjunction with altimetry to separate the thermo-steric part of sea level change from mass change (Lombard et al., 2007; Leuliette and Miller, 2009). In addition, the limited spectral resolution of GRACE and the filtering typically applied in post-processing implies that estimates are affected by nearby mass changes of different physical origin, like GIA and hydrological storage changes in coastal regions. Models of these processes are limited in their ability to represent mass variations and thus to correct the gravity effect in GRACE. For Antarctica, GIA is thought to be the main error source. Another difficulty is that GRACE does not provide the degree-1 harmonic of the mass change, which is important since it causes the center-of-mass of the solid Earth to be displaced in space due to momentum conservation (Rietbroek et al., 2009, 2011).

The fingerprint method suggested by (Plag and Jüttner, 2001; Clark et al., 2002) is based upon the assumption that the major sources of sea level change can be well-modelled in their large-scale spatial characteristics, at least up to a single amplitude for each contribution process (when this assumption is not justified, the source can be subdivided). For these sources, patterns of sea level change (the 'fingerprints') are then computed following the state-of-the-art self-gravitational, elastic theory that includes the rotational feedback of the redistributed ocean mass (Wu and Peltier, 1984; Milne and Mitrovica, 1998). Assembling tide gauge data from a well-distributed network or radar-altimetric sea level allows, in theory, to solve a linear inversion problem for the temporal components. However, several other effects mask those theoretical patterns in the (short) record of data, steric noise being among the more prominent ones.

The fingerprint method can be extended to the analysis of GRACE level 2 products (Stokes coefficients), as we propose in this study. In fact, fingerprints are made up by linear combinations of spherical harmonic coefficients and their estimation thus resembles the 'lumped coefficients' methods in satellite geodesy. In addition to altimetry, GRACE measures over land and therefore the estimation of ice melt fingerprints is stabilized by the direct sensing of mass changes, although one has to include and separate other land signals such as hydrology and GIA as well. Recently, combined self-consistent sea level responses have been calculated from GRACE-derived land loads (Riva et al., 2010).

Another prospect is that, since the fingerprint method essentially transforms the space of the spherical harmonics into a new low-dimensional space of physically consistent base functions with large-scale support, there will be no need for GRACE coefficient filtering or de-striping. This is important, since filtering and rescaling of GRACE solutions (Kusche, 2007) have been recognized as a major source for differences between analyses.

In this study, we have extended the fingerprint method to the simultaneous analysis of Jason-1 altimetry data from the open altimeter database (Schwatke et al., 2010) and GRACE GFZ-RL04 normal equations (Flechtner et al., 2010). Using the sea level equation, we show how self consistent sea level patterns are computed, which parameterize mass changes from ice sheets, land glaciers and hydrology. Additionally, time-space patterns representing steric height changes are collected in a preliminary database (see table 1). We analyse the theoretical resolution and accuracy within this challenging inverse problem and provide a correlation matrix for all estimable parameters. Finally, we solve fingerprint amplitudes from data of the period of 2002-2008, and study the separation of the geocenter motion trend into a present-day mass component and a glacial isostatic adjustment (GIA) contribution.

2. Method

2.1. Sea level fingerprints

The present-day relative sea level change δs, induced by an assumed surface (ice or water storage expressed in equivalent water height) load change δh at time t, is resolved by the sea level equation in the form:

$$\delta s(\lambda,\theta,t) = O(\lambda,\theta)\int_\Omega G^L_{N-U}\left(\delta s(\lambda',\theta',t)+\delta h(\lambda',\theta',t)\right)d\omega + \int_\Omega G^T_{N-U}\delta\Lambda(\delta s,\delta h)d\omega + \frac{\Delta V}{g} \tag{1}$$

In this equation, $O(\lambda,\theta)$ is the ocean function, which is unity at an oceanic location with longitude λ and co-latitude θ and zero elsewhere. The unknown relative sea level is assumed to be in an equilibrium state, in which it has adapted to 1) the gravitational effects of the prescribed (land) load , 2) the change in rotational potential, $\delta\Lambda$, and 3) the gravitational effect of sea level itself. The dependency on the unknown sea level, δs, occurs at both sides of the equality sign but can be solved for by iterative methods or explicitly.

The Greens functions, G^L_{N-U} and G^T_{N-U}, describe the Earth's elastic response to surface loading and tidal loading resp. in terms of the difference between the geoid and the associated uplift (Farrell, 1972). The term $\frac{\Delta V}{g}$ is a uniform shift of the geoid, added to conserve mass of the global surface loading distribution, δT.

$$\int_\Omega \delta T(\lambda',\theta',t)d\omega = \int_\Omega\left(\delta s(\lambda',\theta',t)+\delta h(\lambda',\theta',t)\right)d\omega = 0 \tag{2}$$

In this paper, we will solve the sea level equation in the spectral domain, where we use real-valued fully normalized spherical harmonic base functions[1], $\bar{Y}_{nm}(\lambda,\theta)$, satisfying:

$$\int_\Omega \bar{Y}_{nm}(\omega)\bar{Y}_{n'm'}(\omega)d\omega = 4\pi\delta_{nn'}\delta_{mm'}. \tag{3}$$

Where the base functions are related to the associated Legendre functions, $\bar{P}_{nm}$.

$$\bar{Y}_{nm}(\lambda,\theta) = \begin{cases} \bar{P}_{nm}(\cos\theta)\cos m\lambda, & m \geq 0 \\ \bar{P}_{n|m|}(\cos\theta)\sin m\lambda, & m < 0 \end{cases}$$

[1]no Condon-Shortley phase applied

In the spectral domain, and using the linearized Euler equations, we can write eq. 1 in matrix notation as:

$$\tilde{S} = \mathbf{G}^{L}_{N-U}\left(\mathbf{O}\tilde{S} + \vec{H}\right) + \mathbf{G}^{T}_{N-U}\boldsymbol{\Xi}\left(\mathbf{O}\tilde{S} + \vec{H}\right). \quad (4)$$

Here, $\vec{H}$ is a vector containing the spherical harmonic coefficients of the load δh, expressed in equivalent water height. The boldface symbols $\mathbf{G}^{L/T}_{N-U}$, are the matrix representations of the surface and tidal loading Greens functions in eq. 1. The matrix $\boldsymbol{\Xi}$ maps perturbations of surface loading to changes in the rotational potential, such that total angular momentum of the Earth is conserved.

The multiplication by matrix $\mathbf{O}$ represents the spectral convolution of a function with the ocean function. In a band unlimited domain it will be an infinitely large symmetric projection matrix, whereas the bandlimited case yields a matrix which can be computed analytically, but is not idempotent anymore (Dahlen, 1976; Simons et al., 2006). We computed the matrix $\mathbf{O}$, expressed in geodesy-style normalized spherical harmonics, using Wigner-3j symbols up to degree and order n_{max}=150 and stored the results for reuse. In this study, we construct fingerprints which should be representative for signals covering the last 10 years. During this time period, the shoreline is not expected to change dramatically, and a static Ocean function may therefore be assumed.

The vector $\tilde{S}$ denotes the quasi-spectral sea level (Blewitt and Clarke, 2003; Dahlen, 1976). It represents an equipotential surface, shifted by a uniform constant and its variability is measured with respect to the ocean floor. Since $\tilde{S}$ is non-zero over land we are only allowed to load the Earth with the oceanic component of this function, $\vec{S}$ (which is not an equipotential surface).

$$\vec{S} \equiv \mathbf{O}\tilde{S} \quad (5)$$

2.2. Isotropic Greens functions

For a spherical, nonrotating, elastic and isotropic Earth, with mean radius a, the matrix $\mathbf{G}^{L}_{N-U}$ is diagonal and can be expressed in spectral load Love numbers, h'_n, k'_n.

$$\mathbf{G}^{L}_{N-U} = diag\left\{\frac{3\rho_w}{(2n+1)\rho_e}\left(1 + k'_n - h'_n\right)\right\} \quad ,n > 0 \quad (6)$$

Where, ρ_w and ρ_e is the density of sea water and the mean density of the Earth respectively. Similarly, the matrix $\mathbf{G}^{T}_{N-U}$, convolving tidal (in this case caused by rotation) induced potential is expressed using the body Love numbers, h_n, k_n.

$$\mathbf{G}^{T}_{N-U} = diag\left\{\frac{1}{g}\left(1 + k_n - h_n\right)\right\} \quad ,n > 0 \quad (7)$$

2.3. Rotational feedback

The (sparse) matrix, $\boldsymbol{\Xi}$, maps the degree 2 surface loading coefficients, T_{2m}, to rotational potential changes using three matrix multiplications.

$$\boldsymbol{\Xi} = \underset{\Lambda\leftarrow m}{\boldsymbol{\Phi}} \quad \underset{m\leftarrow J}{\boldsymbol{\Gamma}} \quad \underset{J\leftarrow T}{\boldsymbol{\Psi}} \quad (8)$$

Matrix $\underset{J\leftarrow T}{\boldsymbol{\Psi}}$ relates changes in the rigid Earth's products of inertia, J^R_{i3}, to perturbations in surface loading (Milne and Mitrovica, 1998; Wu and Peltier, 1984).

$$\begin{pmatrix} \delta J^R_{13} \\ \delta J^R_{23} \\ \delta J^R_{33} \end{pmatrix} = \pi a^4 \rho_w \begin{pmatrix} 0 & 0 & -\frac{4}{5}\sqrt{\frac{10}{6}} & 0 \\ 0 & 0 & 0 & -\frac{4}{5}\sqrt{\frac{10}{6}} \\ \frac{8}{3} & -\frac{8}{3\sqrt{5}} & 0 & 0 \end{pmatrix} \begin{pmatrix} T_{00} \\ T_{20} \\ T_{2,1} \\ T_{2,-1} \end{pmatrix} \quad (9)$$

The remaining products of inertia are non-zero but can be ignored as they only occur in higher order terms from the linearized Euler equations (Peltier and Luthcke, 2009; Mitrovica et al., 2005), described by the matrix $\underset{m\leftarrow J}{\boldsymbol{\Gamma}}$:

$$\begin{pmatrix} m_1 \\ m_2 \\ m_3 \end{pmatrix} = \begin{pmatrix} \Omega\frac{1+k'_2}{A\sigma_0} & 0 & 0 \\ 0 & \Omega\frac{1+k'_2}{A\sigma_0} & 0 \\ 0 & 0 & -\frac{1+k'_2}{C} \end{pmatrix} \begin{pmatrix} \delta J^R_{13} \\ \delta J^R_{23} \\ \delta J^R_{33} \end{pmatrix} \quad (10)$$

Here, A and, C, are the Earth's principal moments of inertia, and σ_0 is the Chandler frequency. The symbol Ω denotes the mean frequency of the Earth's rotation. The matrix above models the change in polar motion, m_i, of the elastic Earth subject to an impulse response of changing inertia.

A small rotation of the Earth's axis w.r.t. the observation frame will induce an apparent potential change caused by the misalignment of the centrifugal potential. The matrix, $\underset{\Lambda\leftarrow m}{\boldsymbol{\Phi}}$, maps the polar motion to a change in potential, based on a rigid rotation of spherical harmonics. For general spherical harmonics, the rotation can be performed using the Wigner-D matrix (Wigner, 1960), which redistributes the signal of a coefficient to others having the same degree. In the case of polar motion applied to the centrifugal potential, first order dependencies on m_i propagate to changes in potential as follows:

$$\begin{pmatrix}\Lambda_{00}\\ \Lambda_{20}\\ \Lambda_{2,1}\\ \Lambda_{2,-1}\end{pmatrix} = (a\Omega)^2 \begin{pmatrix} 0 & 0 & \frac{2}{3}\\ 0 & 0 & -\frac{2}{3\sqrt{5}}\\ -\frac{1}{\sqrt{15}} & 0 & 0\\ 0 & -\frac{1}{\sqrt{15}} & 0 \end{pmatrix} \begin{pmatrix} m_1\\ m_2\\ m_3\end{pmatrix} \quad (11)$$

2.4. Solving the Sea level equation

The Greens functions from equations 6, 7 are valid only for degree 1 and upward. The spectral sea level equation (eq. 4) must therefore be augmented by an equation describing the conservation of mass. Since the first (corresponding to degree and order 0) row and column of **O** are simply the spherical harmonic coefficients of the Ocean function, O_{nm}, applying mass conservation in the spectral domain leads to:

$$\vec{S}_{00} = -\vec{H}_{00} = \sum_{n=0}^{n_{max}} \sum_{m=-n}^{n} O_{nm}\tilde{S}_{nm} \quad (12)$$

The mass-induced sea level change can be computed as $\frac{\vec{S}_{00}}{O_{00}}$. Due to the linearization of the Euler equations, and the static coastline, we can now solve eq. 4 for the quasi-spectral sea level and obtain the fully populated sea level Greens function, $\mathbf{G}_{\tilde{S}}$, by inversion.

$$\tilde{S} = \mathbf{G}_{\tilde{S}} \left(\mathbf{G}^{L}_{N-U} + \mathbf{G}^{T}_{N-U}\mathbf{\Xi}\right)\vec{H} = \mathbf{G}_{\tilde{S}}\vec{F}_{N-U} \quad (13)$$

The vector $\vec{F}_{N-U}$ allows for more general forcing to be imposed on the sea level equation, such as for example Earthquake induced loading (Melini et al., 2010).

2.5. Fingerprints database

The linear nature of eq. 13 allows the superposition of diffferent sea level contributors, such as the major ice sheets, land glaciers and remaining terrestrial water storage. We have constructed a preliminary database (see table 1) containing a variety of sea level contributors, with their self-consistent sea level response. In this study, we will produce simplified inversions based on merged fingerprints from the database. With 'merging' we mean an area-weighted average such that the resulting parameter represents an uniform change in the combined subbasins. The drainage basins, considered in Greenland and Antarctica, and land glaciers are plotted in fig. 1. The grouping of the land glaciers will be explained below.

Sea level fingerprints and the associated geoid and sea floor deformation were calculated for uniform changes in the drainage basins of Greenland and Antarctica (taken from Wouters et al. (2008); Horwath and Dietrich (2009)). For the contribution of land glaciers, we have merged the glacier locations from the World Glacier Inventory (WGI) (NSIDC, 1999) and GLIMS (Global Land Ice Measurements from Space) (Raup et al., 2007), using GIS software (GRASS Development Team, 2008). We constructed fingerprints for several important glacier regions such as the Himalayas, Tien Shan, Artic Islands, Alaska, Patagonia, Alps, Caucasus. Within the selected areas each glacier was equally weighted by assigning a point load, which we expressed in spherical harmonics. Each group of glaciers was then normalized to 1 Gton, such that the unknown temporal components have the units Gton. Using this method, we make the assumption that each of the regions glaciers melts at the same rate although the actual melting rates may well be different. However, since the melting rates for each glacier are for a large part unknown and may be inaccurate, we believe that our approach is appropriate. In any case, it provides adequate information about the spatial distribution of the glaciers. Furthermore, sub-regions with a concentration of glaciers will automatically contribute more to the sea level. To supress high resolution Gibbs phenomena, associated with our finite truncation, we have additionally applied a 200 km half width Gaussian filter to the patterns before normalization.

The sea level fingerprints of terrestrial water storage were accounted for by 9 (complex or real) empirical orthogonal functions (EOF, Preisendorfer and Mobley (1988)), derived from the WaterGAP Global Hydrology Model (WGHM) (Döll et al., 2003). These 9 real and complex modes explain 85% and 92% of the modeled WGHM signal respectively. Within the inversion, the patterns of the EOF are assumed to be fixed while the time varying principal components of these patterns are freely estimated.

For the parameterization of the steric sea level, sensed by altimetry, we used 9 EOFs computed from the steric sea level from Ishii et al. (2006). It must be noted that the steric sea level from Ishii et al. (2006) only represents changes in the upper 700 meters of the ocean. More advanced parameterizations incorporating the ocean response to melting using the Finite Element Sea-Ice Ocean model (FESOM, Timmermann et al. (2009)) are being investigated (Brunnabend et al., 2011, this issue), but are not considered in this study.

The geoid and sea level will also exhibit secular changes from glacial isostatic adjustment (GIA). As a GIA fingerprint we have used the present-day trend from the GIA model by Klemann and Martinec (2009), forced by ICE5G (VM2) (Peltier, 2004). In order to correct the modelled GIA pattern for errors we estimate a single amplitude, which will be unity for an errorless model. This approach does not correct the model regionally, but this is currently outside the scope of this paper. Care has been taken to express the GIA pattern in the Center of Figure (CF) frame of the Earth, such that it is consistent with the other patterns.

We currently do not account for changes in ocean dynamic topography, as measured by satellite altimetry. This requires the assumption that the remaining signal from the dynamic topography will propagate as noise in the altimetry residuals after fitting. In the results section altimetric residuals, remaining after removing the joint inversion results, are discussed in more detail. The mean dynamic topography is accounted for by using sea level anomalies as altimeter measurements.

2.6. GRACE gravimetry

Since 2002, changes in the Earth's gravitational potential are accurately measured by the GRACE satellite twins (Tapley et al., 2004). The unknown amplitudes of the self consistent fingerprints, $\vec{x}$, can be linked to changes in (weekly or monthly) Stokes coefficients, $\delta\vec{\Phi}$, as measured by GRACE.

$$\delta\vec{\Phi}(t) = \mathbf{A}(t)\begin{pmatrix}\vec{x}_{ice}\\ \vec{x}_{glac}\\ \vec{x}_{hydro}\\ \vec{x}_{gia}\end{pmatrix} + e \qquad (14)$$

The design matrix, **A**, consist of columns which represent the 1 Gton normalized fingerprints in terms of potential change. The time dependency in **A** arises from the columns associated with the GIA fingerprint, which varies secularly over time. The error, e, contains the GRACE errors. We constructed normal equations expressed in the unknown amplitudes for running means of 11 GPS weeks, from the GFZ release 04 normal equations (Flechtner et al., 2010). The period of 11 weeks was chosen such that sub-annual signal can still be adequately represented, while averaging out high frequency phenomena. Using an odd number of 11 weeks also ensures that the center time of each running mean is still aligned to the GPS weeks. For purposes related to the estimation of the static gravity field, those normal equations are stored up to degree and order 150. Without the need for intermediate inversion, we can take advantage of the available resolution and convert the full normal equations in terms of fingerprint amplitudes, by using **A**. In order to be consistent with the altimetry, the weekly atmospheric and oceanic contribution, as well as the convential rates in C_{20} and C_{40}, are restored. To be consistent with the IB-correction from altimetry, we do not restore the oceanic average of the atmosphere over the ocean (Leuliette and Miller, 2009).

2.7. Jason-1 altimetry

An altimeter essentially measures the mass contribution to geocentric sea level, the steric height changes due to temperature and salinity variations and dynamic topography. An along-track sea level anomaly, δh_{sla} can be related to the unknown fingerprint amplitudes similar to eq. 14.

$$\delta h_{sla}(t) = \mathbf{B}(t)\begin{pmatrix}\vec{x}_{ice}\\ \vec{x}_{glac}\\ \vec{x}_{hydro}\\ \vec{x}_{gia}\\ \vec{x}_{ster}\end{pmatrix} + e \qquad (15)$$

The design matrix **B** contains columns which are the fingerprints propagated to the measurement locations, using spherical harmonic analysis. In this study we have used Jason-1 (Chambers et al., 2003) data from the Open Altimeter Database (OpenADB) (Schwatke et al., 2010). In addition to the standard range corrections (including the inverse barometer correction), the data has also been corrected for radial orbit errors. Altimeter ranges have been sorted and interpolated to predefined bins, which remain fixed in time and space. This has the advantage that the fingerprints used in matrix **B**, only need to be calculated once. We have selected Jason-1 measurements over the ocean batched in GPS weeks to align them with the available GRACE data. Normal equation systems for an 11 week running mean were subsequently constructed with the altimeter range errors as a diagonal error covariance matrix.

The self consistent sea level varies strongest in the vicinity of the mass source. High latitude altimeter measurements are therefore the most sensitive to Greenland and Antarctica mass changes. Unfortunately, Jason-1 measurements are restricted to ±66° and the higher latitude measurements are strongly biased by signals from floating sea ice. To prevent the contamination of the data by sea ice, we have excluded all measurements falling within the region of maximum sea ice extent. We also suspect that a time varying sea ice extent might cause an unwanted aliasing effect as near field measurements are then essentially sampled once a year only.

2.8. Conservation of linear momentum

Through the conservation of linear momentum, the fitted surface loading phenomena are accompanied by a motion of the geocenter. This is the relative movement of the center of mass (CM) of the complete Earth system in the center of figure (CF) frame, which approximates the center of Earth (CE) frame (Blewitt and Clarke, 2003). After estimating the temporal components of ice sheets, glaciers, hydrology and the trend correction in GIA, one can calculate the resulting geocenter motion. Here, we use an alternative method, where we augment the normal equations with three unknowns (the cartesian components of the geocenter motion $\vec{r}_{CF}$). Since the geocenter motion in the CM frame is zero per definition we may use those as zero valued pseudo observations (accuracy is assumed to be 0.1 mm) in an additional normal system, by implementing the following observation equation:

$$a\sqrt{3}[\mathbf{A}]_{n=1}\begin{pmatrix}\vec{x}_{ice}\\ \vec{x}_{glac}\\ \vec{x}_{hydro}\\ \vec{x}_{gia}\end{pmatrix} - \vec{r}_{CF} + e = \vec{r}_{CM} = \vec{0} \qquad (16)$$

The design matrix $[\mathbf{A}]_{n=1}$, is a sub matrix from that in eq. 14, and comprises the fingerprint degree 1 components in the appropriate CF frame. It is convenient to bind the geocenter motion to the normal systems, since it can be estimated at once together with the other parameters and the robustsness of the inversion against apriori geocenter motion can be easily tested.
Each fingerprint comes with a fixed direction of its associated geocenter motion, making it possible to retrieve $\vec{r}_{CF}$ from GRACE-only normal systems as well.

3. Results

3.1. Errors and separability

We have assessed the ability of parameter seperation of a joint Jason-1 and GRACE inversion. For that means we have extracted from the fingerprint database a simplified subset of patterns. We chose 9 EOF patterns for both the steric and hydrological component. Land glacier contribution is parameterized by 6 globally distributed components from 1) Alaska, 2) the Artic islands, 3) Patagonia, 4) the Alps and the Caucasus, 5) Himalaya and Tien Shan and 6) Kamchatka. Estimated parameters represent 11 week running means, except for the GIA intersect and trend, which is constrained using data from the complete period (2003-2008).

We have plotted the formal error correlation matrix in fig. 2, which illustrates how GRACE and Jason-1 errors propagate into our estimates. The strongest (negative) correlations (< -0.9) exists between the high and low elevation (split at the 2000 m contour) components of drainage basins. This effect is most apparent for the Greenland ice sheet, containing small sized subbasins, and to a lesser extent for the Antarctic ice sheet.

The steric parameters display weaker error correlations compared to the hydrological parameters. We attribute this to the accurate and fine sampling of Jason-1 data, which allows detailed structures to be resolved over the ocean compared to GRACE over land.

The magnitude of the formal errors are plotted in figure 3. These errors are generally too optimistic, as non-fitted signal is not regarded as noise, but they provide lower bounds for obtainable estimates. Furthermore, relative errors between the parameters can be compared. A simplified Jason-1 only inversion, with merged patterns for Greenland, Antarctica and the land glaciers, is additionally shown. When we calculate the posteriori fit of the data, we find posteriori sigma scaling factors varying over the period between 1.05 and 1.20 for the joint inversion. This means that joint inversion errors will be approximately 5-20% larger (for the plot in Fig. 3 the scaling factor was found to be 1.14).

We find that GRACE data determine the accuracy of virtually all of the mass related parameters. The steric parameters are well resolved by the addition of Jason-1 data with lowest formal accuracies in the order of 0.01 mm global sea level height. Although, the mass related parameters are weakly determined for a Jason-1 only inversion, we see that the accuracy of the steric amplitudes is only marginally affected by the solution space of the mass related parameters.

The drainage basins with the largest uncertainties, $\sim$40 Gton, are the high elevation Greenland drainage basins in Southern Greenland (number 5 and 6). The errors of the two parameters are highly correlated ($\rho = -0.95$, see fig. 2), since the associated fingerprints are very similar and the considered areas are relatively small. Based on the propagation of GRACE errors in those basins, Wouters et al. (2008) found errors in their trend, ranging in the order of 5-6 $^{\mathrm{Gton}}/_{\mathrm{yr}}$. When propagated to trends, our errors would yield smaller errors of 2-3 Gton/yr for the same basins.

Compared to Greenland, the 6 land glaciers contributions can be resolved better with accuracies in the 2-3.5 Gtons range. This can be mainly attributed to the large distances between the glacier locations, resulting in spatially distinct fingerprints.

3.2. Geocenter motion and glacial isostatic adjustment

In a scheme using real data we have constructed an inversion where we merged the high and low elevation parts of the drainage basins. Figure 6 shows the total estimated geocenter motion variation, together with trends from the present-day variation and the contribution from GIA. The GIA trend correction from the joint inversion is estimated to be 1.16 (1.0 meaning no correction), whereas a GRACE only inversion, over the same period, resulted in a correction factor of 0.92.

The Z component of the geocenter motion varies most strongly both in trends and in terms of seasonal behavior. Recently, Wu et al. (2010) also estimated the GIA and present-day mass (PDM) contribution to geocenter motion trends, using GRACE (CSR), GPS and ocean bottom pressure from the ECCO model. For Z, the GIA contribution agrees closely with that of Wu et al. (2010) (-0.72 mm/yr vs. -0.71 mm/yr), while our PDM component shows a stronger trend (-0.37 mm/yr versus -0.16 mm/yr). Our X component trend (-0.14 mm/yr for both PDM and GIA) is slightly larger than that estimated by Wu et al. (2010) (PDM: -0.08 mm/yr, GIA: -0.1 mm/yr). Furthermore, although we find a good agreement in the overall trend for Y (Wu et al. (2010): 0.4 mm/yr, this study: 0.43 mm/yr), the contribution of the PDM versus GIA is reversed.

3.3. Altimetric sea surface height residuals

In the setup above, we have represented the steric sea surface height (SSH) changes by only 9 EOF patterns. As mentioned before, the patterns were obtained from temperature and salinity measurements of the upper part (700 m) of the ocean. Nevertheless, the principal components (PC's) from the original EOF analysis may be compared to the fitted PC's from the inversion (see figure 4). The principal components are normalized such that their magnitude represents the uniform contribution to sea level rise. Although warming/cooling from the deeper ocean might be present in the fitted PC's, we find a good agreement. This indicates that the interannual signal is well represented in both datasets and that steric changes in the deeper ocean have only a limited influence on the estimated amplitudes.

In order to investigate the SSH residuals which remains after the joint inversion, we have propagated the inversion results (steric patterns, sea level changes due to the ice sheets/glaciers/hydrology and GIA) to along-track Jason-1 data. For each along-track bin we have calculated the variability over the period of the inversion. The along-track variability before and after removing the fit are shown in Fig. 5. Clearly, the inversion removes large scale signals in the Pacific, Atlantic and Indian Ocean. As expected, regions with large variations in dynamic topography (Kuroshio, Gulf, Agulhas), display virtually no reduction. Fig. 5 also shows remaining signal in the equatorial Pacific and Indian Ocean, indicating remaining Rossby waves. Since these are mainly shallow phenomena, we expect that, in future research, increasing the amount of fitted steric EOF's may additionally absorb those signals.

4. Conclusion

The potential of a joint altimetry and GRACE inversion in terms of sea level fingerprints has been demonstrated for the first time. We have constucted a preliminary fingerprint database, containing self-consistent equilibrium sea level responses to forcings from ice sheets, land glaciers and hydrological signals. Furthermore, the database currently also contains a steric representation based on an EOF decomposition of the upper 700 m ocean and a pattern involving GIA signal. Within the inversion, the pattern of each signal is known while the temporal amplitude can be freely estimated.

We find that the GRACE data mostly determines the accuracy of the mass related parameters, such as glacier and ice sheet changes, and hydrology. While altimetry has only a marginal capability to resolve these mass related parameters, the steric height changes in the ocean can be adequately resolved. When GRACE and altimetry errors are propagated to the unknowns, we find strong negative error-correlations mainly between high and low elevation parts of the drainage basins. In Greenland we found maximum formal errors of ~40 Gtons for small and neighbouring basins. The accuracy of the individual basin components is determined by the size and similarity of the corresponding fingerprints. In addition, since GRACE is most sensitive to along-track gravity changes, the orientation of the basins may also play a role.

In a first inversion experiment, we have investigated the separability of the present-day and glacial isostatic components in the geocenter motion. We find a general agreement with the results of Wu et al. (2010), although discreprancies remain in the present-day Z component and the relative distribution of GIA and PDM in the Y component.

After propagating the joint inversion results to along-track altimetry, Jason-1 residuals have been investigated. We found that the inversion results reduce the variability of the residuals, mainly on large scales. Some signal remains, which may be fitted using additional or alternative representations in future research. Other signals, such as those associated with regions of strongly varying dynamic ocean topography, are not expected to be reduced, by adding more patterns. These have to be either reduced using a priori corrections, or should be treated as noise and be expected to average out over longer time scales.

The fitted principal components, associated with the steric EOF's, compare well with the ones derived from ARGO floats (Ishii et al., 2006), although these are confined to the upper ocean only. Therefore the agreement indicates that, for those 9 EOF's, the deeper ocean (below 700 m) plays a marginal role in terms of steric height. The influence of the deeper ocean may become apparent in either the cumulative effect of the fitted modes or in remaining data residuals.

The current study knows some limitations, which should be addressed in the future. The steric patterns as derived from Ishii et al. (2006) have no direct coupling with the actual ice sheet changes and extend only to a depth of 700 m. Current simulation efforts yielding more advanced sea level responses to melting are underway (Brunnabend et al., 2011, this issue). We expect that the contribution of altimetry to the estimation of mass related parameters will be improved with those parameterizations. The associated patterns show typical high resolution fingerprints over the ocean, which can be adequately resolved by altimetry.

In the present setup, the patterns have been assumed to be static, while the amplitudes are allowed to vary in time. The assumption of sea level and ocean bottom pressure responding linearly to forcings may break down when one tries to extrapolate the inversion results backward or forward in time. In future research, we plan to test this linearity assumption by applying a backward extrapolation of the inversion results and comparing those with historical tide gauges.

Currently, the representation of the glacial isostatic adjustment process involves a single pattern and rate. More advanced representations are desirable, which allow a parameterization of a wider spectrum of realistic GIA models arising from variations in ice history and Earth viscosity.

Acknowledgments

We would like to thank Christoph Dahle and Frank Flechtner for providing the full GRACE normal equations. The GIA patterns were kindly provided by Volker Klemann. Additionally, the binning of Jason-1 data and orbit corrections have been prepared by Roman Scavenko and Christian Schwatke. Wigner 3-j symbols were calculated using software from the SHTOOLS package from Marc Wieczorek. The authors acknowledge support under grants KU 1207/9-1 and SCHR779/6-1 in the framework of the German priority program SPP1257: Mass transport and mass distribution in the system Earth. Finally, we thank two anonymous reviewers for their time on reviewing the manuscript.

References

Bindoff, N., Willebrand, J., Artale, V., Cazenave, A., Gregory, J., Gulev, S., Hanawa, K., Le Quere, C., Levitus, S., Nojiri, Y., et al., 2007. Observations: oceanic climate change and sea level in Climate Change 2007: The Physical Science Basis. Contribution of Working Group I to the Fourth Assessment Report of the Intergovernmental Panel on Climate Change. Cambridge University Press.

Blewitt, G., Clarke, P., 2003. Inversion of earth's changing shape to weigh sea level in static equilibrium with surface mass redistribution. Journal of Geophysical Research (Solid Earth) 108, 2311.

Brunnabend, S.E., Schröter, J., Timmermann, R., Rietbroek, R., Kusche, J., 2011. Modeled steric and mass-driven sea level change caused by greenland ice sheet melting. Journal of Geodynamics (in press) .

Cazenave, A., Llovel, W., 2010. Contemporary sea level rise. Annual Review of Marine Science 2, 145–173.

Chambers, D.P., Ries, J.C., Urban, T.J., 2003. Calibration and verification of jason-1 using global along-track residuals with topex special issue: Jason-1 calibration/validation. Marine Geodesy 26, 305–317.

Clark, P.U., Mitrovica, J.X., Milne, G.A., Tamisiea, M.E., 2002. Sea-level fingerprinting as a direct test for the source of global meltwater pulse ia. Science 295, 2438.

Cogley, J.G., 2009. Geodetic and direct mass-balance measurements: comparison and joint analysis. Annals of Glaciology 50, 96.

Dahlen, F.A., 1976. The passive influence of the oceans upon the rotation of the earth. Geophysical Journal of the Royal Astronomical Society 46, 363–406.

Döll, P., Kaspar, F., Lehner, B., 2003. A global hydrological model for deriving water availability indicators: model tuning and validation. Journal of Hydrology 270, 105–134.

Farrell, W.E., 1972. Deformation of the earth by surface loads. Reviews of Geophysics and Space Physics 10, 761.

Flechtner, F., Dahle, C., Neumayer, K.H., König, R., Förste, C., 2010. The release 04 champ and grace eigen gravity field models. System Earth via Geodetic-Geophysical Space Techniques, Adv. Technologies in Earth Sciences , 41.

GRASS Development Team, 2008. Geographic Resources Analysis Support System (GRASS GIS) Software. Http://grass.osgeo.org.

Horwath, M., Dietrich, R., 2009. Signal and error in mass change inferences from grace: the case of antarctica. Geophysical Journal International 177, 849.

Ishii, M., Kimoto, M., Sakamoto, K., Iwasaki, S.I., 2006. Steric sea level changes estimated from historical ocean subsurface temperature and salinity analyses. Journal of Oceanography 62, 155.

Klemann, V., Martinec, Z., 2009. Contribution of glacial-isostatic adjustment to the geocenter motion. Tectonophysics (online first, doi:10.1016/j.tecto.2009.08.031) .

Kusche, J., 2007. Approximate decorrelation and non-isotropic smoothing of time-variable grace-type gravity field models. Journal of Geodesy 81, 733.

Leuliette, E.W., Miller, L., 2009. Closing the sea level rise budget with altimetry, argo, and grace. Geophysical Research Letters 36, –04608.

Llovel, W., Becker, M., Cazenave, A., Crétaux, J.F., Ramillien, G., 2010. Global land water storage change from grace over 2002–2009; inference on sea level. Comptes Rendus Geosciences 342, 179–188.

Lombard, A., Garcia, D., Ramillien, G., Cazenave, A., Biancale, R., Lemoine, J.M., Flechtner, F., Schmidt, R., Ishii, M., 2007. Estimation of steric sea level variations from combined grace and jason-1 data. Earth and Planetary Science Letters 254, 194–202.

Melini, D., Spada, G., Piersanti, A., 2010. A sea level equation for seismic perturbations. Geophysical Journal International 180, 88–100.

Milne, G.A., Mitrovica, J.X., 1998. Postglacial sea-level change on a rotating earth. Geophysical Journal International 133, 1–19.

Mitrovica, J.X., Tamisiea, M.E., Davis, J.L., Milne, G.A., 2001. Recent mass balance of polar ice sheets inferred from patterns of global sea-level change. Nature 409, 1026–9.

Mitrovica, J.X., Wahr, J., Matsuyama, I., Paulson, A., 2005. The rotational stability of an ice-age earth. Geophysical Journal International 161, 491–506.

NSIDC, 1999. Word glacier inventory (updated 2009). World Glacier Monitoring Service and National Snow and Ice Data Center/World Data Center for Glaciology. Boulder, CO. Digital media.

Peltier, W., 2004. Global glacial isostasy and the surface of the ice-age earth: The ice-5g (vm2) model and grace. Annual Review of Earth and Planetary Sciences 32, 111.

Peltier, W.R., Luthcke, S.B., 2009. On the origins of earth rotation anomalies: New insights on the basis of both "paleogeodetic" data and gravity recovery and climate experiment (grace) data. Journal of Geophysical Research 114, B11405.

Plag, H.P., Jüttner, H.U., 2001. Inversion of global tide gauge data for present-day ice load changes. Mem Natl Inst Polar Res Spec Issue 54, 301–317.

Preisendorfer, R.W., Mobley, C.D., 1988. Principal component analysis in meteorology and oceanography. Developments in Atmospheric Science 17, Elsevier, Amsterdam.

Raup, B., Racoviteanu, A., Khalsa, S., Helm, C., R, A., Arnaud, Y., 2007. The glims geospatial glacier database: A new tool for studying glacier change. Global and Planetary Change 56, 101.

Rietbroek, R., Brunnabend, S., Dahle, C., Kusche, J., Flechtner, F., Schröter, J., Timmermann, R., 2009. Changes in total ocean mass derived from grace, gps, and ocean modeling with weekly resolution. Journal Of Geophysical Research-Oceans 114, C11004.

Rietbroek, R., Fritsche, M., Brunnabend, S.E., Daras, I., Kusche, J., Schröter, J., Flechtner, F., Dietrich, R., 2011. Global surface mass from a new combination of grace, modelled obp and reprocessed gps data. Journal of Geodynamics In Press, Corrected Proof.

Riva, R.E.M., Bamber, J.L., Lavallée, D.A., Wouters, B., 2010. Sea-level fingerprint of continental water and ice mass change from grace. Geophysical Research Letters 37, L19605.

Schwatke, C., Bosch, W., Savcenko, R., Dettmering, D., 2010. Openadb: An open database for multi-mission altimetry. EGU Geophysical research abstracts, http://openadb.dgfi.badw.de .

Simons, F.J., Dahlen, F.A., Wieczorek, M.A., 2006. Spatiospectral concentration on a sphere. SIAM Rev. 48, 504–536.

Stammer, D., 2008. Response of the global ocean to greenland and antarctic ice melting. Journal of Geophysical Research (Oceans) 113, C06022.

Tamisiea, M.E., Mitrovica, J.X., Milne, G.A., Davis, J.L., 2001. Global geoid and sea level changes due to present-day ice mass fluctuations. Journal of Geophysical Research 106, 30849.

Tapley, B.D., Bettadpur, S., Ries, J.C., Thompson, P.F., Watkins, M.M., 2004. Grace measurements of mass variability in the earth system. Science 305, 503–506.

Timmermann, R., Danilov, S., Schröter, J., Böning, C., Sidorenko, D., Rollenhagen, K., 2009. Ocean circulation and sea ice distribution in a finite element global sea ice-ocean model. Ocean Modelling 27, 114–129.

Wigner, E.P., 1960. Group theory and its application to the quantum mechanics of atomic spectra. American Journal of Physics 28, 408–409.

Willis, J.K., 2010. Can in situ floats and satellite altimeters detect long-term changes in atlantic ocean overturning? Geophysical Research Letters 37, L06602.

Wouters, B., Chambers, D., Schrama, E.J.O., 2008. Grace observes small-scale mass loss in greenland. Geophysical Research Letters 35, L20501.

Wu, P., Peltier, W.R., 1984. Pleistocene deglaciation and the earth's rotation: a new analysis. Geophysical Journal of the Royal Astronomical Society 76, 753–791.

Wu, X., Heflin, M.B., Schotman, H., Vermeersen, B.L.A., Dong, D., Gross, R.S., Ivins, E.R., Moore, A.W., Owen, S.E., 2010. Simultaneous estimation of global present-day water transport and glacial isostatic adjustment. Nature Geoscience 3, 642.

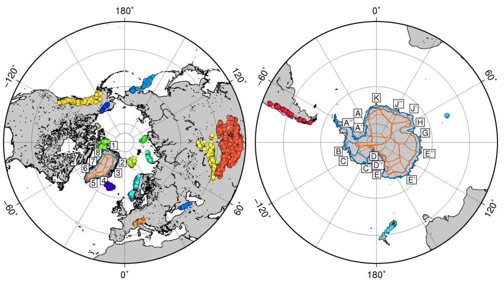

Figure 1: Greenland and Antarctic ice sheet drainage basins and clustered land glaciers, contained in the fingerprint database. The Greenland and Antarctic basin tags follow that of Wouters et al. (2008) and Horwath and Dietrich (2009) respectively. The glacier locations come from the World Glacier Inventory (WGI) and GLIMS.

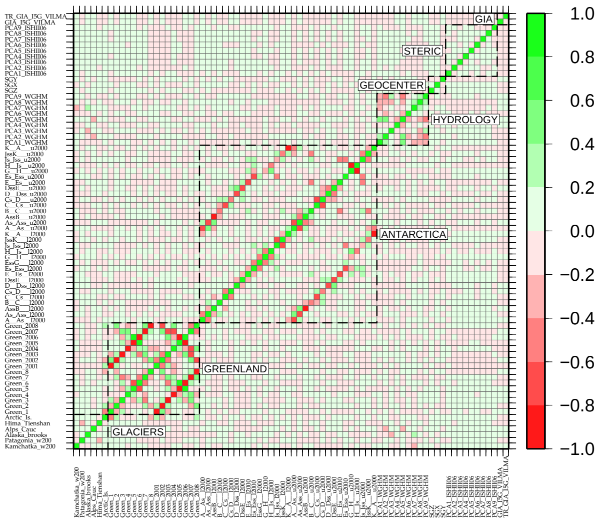

Figure 2: Error-correlation matrix of a 11 week running mean Jason-1 + GRACE combination centered on GPS week 1500 (08-10-2008). The GIA parameters (intersect and trend) are constrained using the complete dataset. The Greenland and Antarctic drainage basins are divided at the 2000 m height contour in an upper and lower part. Hydrology and steric changes are each parameterized by 9 principal components. The contribution of land glaciers is simplified to 6 main contributors. Relative strong negative correlations exist between lower and upper elevation parts of the drainage basins. Steric parameters appear to be well separable, which can be attributed to the Jason-1 data. Weak correlations exist between the estimated hydrological parameters.

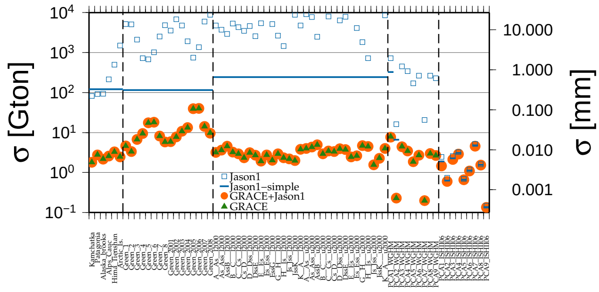

Figure 3: Formal parameter errors (GPS week 1500) expressed in Gton/uniform sea level change for GRACE only, Jason-1 only and combination inversions. Whereas the errors of the mass related parameters for the joint inversion are constrained by GRACE, Jason-1 effectively constrains the steric parameters even though the mass parameters are weakly determined (note the logarithmic Y axis). The simplified Jason-1 inversion has merged parameters for Greenland, Antarctica and the land glaciers. For all inversions, the GIA parameters are constrained using the full combination solution.

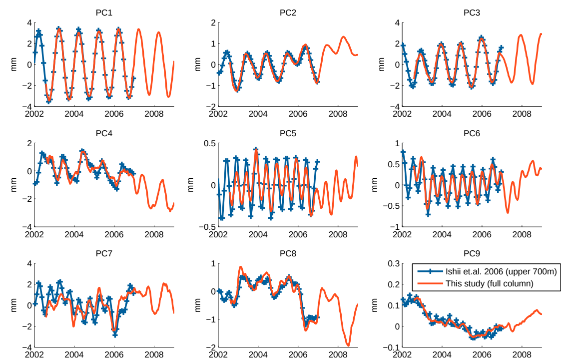

Figure 4: The first 9 principal components of steric heights derived from the Ishii et al. (2006) dataset (blue line with '+'s) versus those as estimated from the joint inversion (solid red line). The principal components are scaled such that the vertical scale represents the uniform contribution of the corresponding mode to global sea level. For example, the first mode causes a seasonal variation of ~ 3 mm in terms of uniform sea level rise. The discrepancies between the curves may be explained by remaining errors in the ARGO data and/or the contribution of the deeper ocean in the joint inversion results.

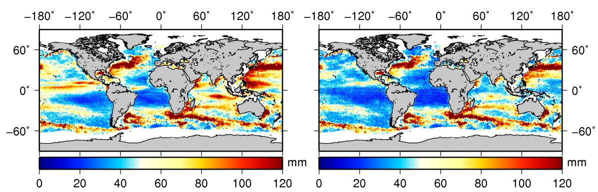

Figure 5: Left: Variability of the Jason-1 along-track measurement bins before fitting (a running mean of 11 weeks has been applied in order to be consistent with the inversion results). Right: variability of the Jason-1 residuals after removing the joint inversion results. After fitting, reductions can be seen in the Pacific, Indian and Atlantic Ocean, while regions with high variability in dynamic topography (Gulf stream, Kuroshio, Agulhas) display little change.

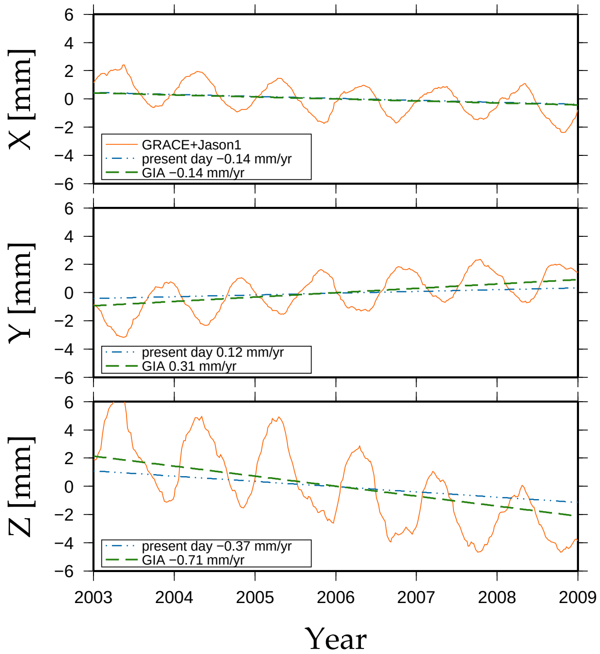

Figure 6: Estimated geocenter motion from a GRACE+Jason-1 combination over the period 2002-2008. The associated trend has been separated into a present-day component and a GIA component.

Contributing process	# regions	Timescale	Model/reference	observable
Greenland	16	seasonal-interannual	Wouters et al. (2008)	N,U,S
Antarctica	31	seasonal-interannual	Horwath and Dietrich (2009)	N,U,S
Glaciers	16	seasonal-interannual	WGI/GLIMS	N,U,S
Hydrology	9 (EOF's)	weekly-seasonal	WGHM (Döll et al., 2003)	N,U,S
Hydrology	9 (CEOF's)	weekly-seasonal	WGHM (Döll et al., 2003)	N,U,S
GIA	1(global)	secular	VILMA (ICE5g+VM2) (Klemann and Martinec, 2009)	N,U,S
Steric	9 (EOF's)	monthly-interannual	Ishii et al. (2006)	Steric S
Steric	9 (CEOF's)	monthly-interannual	Ishii et al. (2006)	Steric S
Circulation	-	daily-interannual	FESOM (planned)	Dyn. Topo./steric S

Table 1: Preliminary fingerprint inventory. N, U, and S denote geoid change, uplift and sea level respectively.